

Short-range depinning in the presence of velocity-weakening

Tom W.J. de Geus¹, Matthieu Wyart^{1,2}

¹*Institute of Physics, École Polytechnique Fédérale de Lausanne (EPFL), Switzerland*

²*Department of Physics and Astronomy, Johns Hopkins University, Baltimore, MD, USA*

November 12, 2024

Abstract

Phenomena including friction and earthquakes are complicated by the joint presence of disorder and non-linear instabilities, such as those triggered by the presence of velocity weakening. In [1], we provided a theory for the nucleation of flow and the magnitude of hysteresis, building on recent results on disorder-free systems described by so called rate-and-state descriptions of the frictional interface, and treating disorder perturbatively. This theory was tested for models of frictional interfaces, where long range elastic interactions are present. Here we test it for short-range depinning, and confirm that (i) nucleation is triggered by avalanches, governed by a critical point at some threshold force f_c close to the minimum of the flow curve and that (ii) due to an armouring mechanism by which the elastic manifold displays very little plasticity after a big slip event, very slowly decaying finite size effects dominate the hysteresis magnitude, with an exponent we can relate to other observables.

1 Introduction

Elastic interfaces pinned by disorder are found in various systems, including crack fronts in fracture [2], frictional interfaces [3], domain walls in magnets [4, 5], sliding charge density waves [6] or vortex lattices in superconductors [7]. In the absence of temperature, the interface is pinned by impurities, but undergoes a *depinning transition* [8–10] at some critical force (or stress, or magnetic field). When inertia is not present, the physics is well-understood: the interface moves via large reorganizations called avalanches, and the velocity of the interface grows above the depinning threshold where it vanishes with some critical exponent.

In other systems, such as frictional interface [11, 12], crack fronts in brittle materials [13] or wetting on rough solid surfaces [14, 15], a sufficient inertia or other effects can induce the flow curve to be non-monotonic [16–18]. Indeed, in the presence of inertial effects, flow generates acoustic waves, that can make it easier to jump over local barriers induced by disorder, in turn accelerating flow. Such positive feedback can lead to velocity-weakening as sketched in Fig. 1a, causing instabilities and stick-slip. How such instabilities are triggered as the force is slowly increased is a central question to various fields, including earthquake science and tribology. Understanding it remains a theoretical challenge, as one needs to deal both with disorder and the presence of non-linear instabilities. This question relates to what controls the magnitude of hysteresis effects apparent when comparing the starting point

of the flow upon increasing the applied load to its stopping point upon decreasing it again.

At least three scenarios have been proposed for how the depinning transition is affected by inertia:

Scenario A: The depinning transition becomes first order as soon as inertia is present. For a finite amount of inertia, motion is triggered by small avalanches, and the hysteresis loop is of finite magnitude in the thermodynamic limit. This picture was obtained by treating inertia as a perturbation around the usual depinning behaviour [19]. It does not occur in mean-field [16] nor in more recent numerical observations [17, 18, 20, 21], where for mild inertial effects evidence of a continuous transition exists.

Scenario B: For small inertia, the flow curve is still monotonic with some modified threshold force f_c^\downarrow [22]. Flow is critical at f_c^\downarrow , and in the same universality class as when inertia is absent. The hysteresis loop vanishes in the thermodynamic limit, but very slowly, due to a combination of two effects. First, nucleation of flow emerges from rare avalanches exceeding a size $\ell_c \sim (f - f_c^\downarrow)^{-\tilde{\nu}}$, where $\tilde{\nu}$ is a critical exponent characterizing the depinning transition in the absence of inertia. Second, only rare sites can yield under loading after a slip event and trigger an avalanche. Limitations of this approach are the following. *Limitation B1:* It was supported by an automaton model where inertia is modelled as a brief overshoot of the force change in sites surrounding rearrangements. In [23], it was argued that for more generic automaton models, a

finite hysteresis should be present, while flow is still governed by a continuous transition at f_c^\downarrow . These results indicate the need to go beyond automaton models and model inertia more accurately. *Limitation B2*: This approach focused on small inertial effects, and did not capture macroscopic velocity weakening. *Limitation B3*: The nucleation picture could not be tested precisely because in systems of limited size, flow is triggered far from f_c^\downarrow .

Scenario C: In a recent work [1], we addressed these limitations and focused on the case where velocity weakening is present (thus *scenario C* needs not contradict *scenario B*, as these could each apply at different levels of inertial effect or damping coefficient). We built on the rate-and-state description of homogeneous frictional interfaces which includes from the start velocity weakening of the interface [24, 25], and treat *disorder* perturbatively. A result of the rate-and-state literature [26, 27] central to our approach is pictured in Fig. 1: for a pure system, there exists a threshold force f_c (very) slightly above the minimum f_{\min} of the flow curve $v(f)$, where a frictional interface can be destabilized and rupture – a result that holds both for short and long-range elastic interactions [27]. In [1], we argued that in the presence of disorder, f_c controls nucleation, triggered by avalanches whose extension goes beyond some length:

$$\ell_c(f) \sim (f - f_c)^{-\nu}. \quad (1)$$

The exponent ν in the presence of velocity-weakening differs from $\tilde{\nu}$ observed in its absence. Nucleation is revealed by a bimodal distribution of event sizes¹, corresponding of both avalanches and system-spanning events, as sketched Fig. 2c. Thus, nucleation from the static phase is controlled by a critical point at f_c , as pictured in Fig. 2. In this scenario, there exists a tiny finite hysteresis in the thermodynamic limit because $f_c > f_{\min}$, as illustrated in Fig. 1. The flow regime, by contrast, displays a first order transition when the load is reduced.

In this scenario, the hysteresis magnitude displays very slowly decaying finite size effects, for reasons similar to those put forward in *scenario B* and [22] (except that hysteresis magnitude does not decay to zero as $f_c > f_{\min}$). In particular, after a large slip event, the system is depleted of weak regions about to trigger an avalanche (i.e. “yield”). The density of such regions was argued to vanish at a small local yield threshold x as a power law $P(x) \sim x^{\theta'}$ in [29, 30], an effect we called “armouring” of the interface. Such a power-law distribution

is referred to as pseudo-gap in the literature [31, 32]. It leads to a scaling law for the excess hysteresis magnitude as a function of system size.

These results were tested in [1, 29] using a finite element model where inertia is treated by actually solving Newton’s equation, and where disorder is modelled with a random potential acting on each element, inspired by a previous model by Jagla [33]. A central idea to test this picture of nucleation was to trigger avalanches at various force levels² [29], as the spontaneous triggering of avalanches under loading around f_c is too rare to allow for statistical analysis. These studies focused on long-range interactions, where additional effects (such as “radiation damping”) make this scenario slightly more complicated to test.

In the present work, we test *scenario C* for a one dimensional elastic line pinned by disorder, with short-range elastic interactions. We first verify our prediction on nucleation in Eq. (1), which requires both to access the non-monotonic flow curve, used to extract f_c (approximated as f_{\min}), as well as to study the statistics of avalanches artificially triggered at different forces along the stick-slip cycle. Secondly, we confirm our predictions for how the magnitude of the hysteresis cycle depends on system size. Thereto, we combine the avalanche and nucleation properties with the density of regions about to yield, $P(x)$, through the associated pseudo-gap exponent.

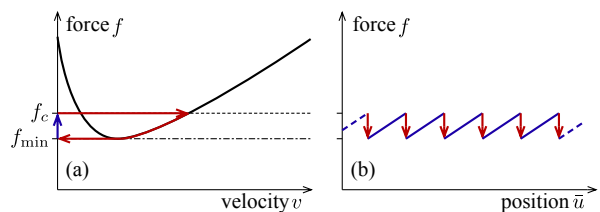


Figure 1. [Sketch] (a) When the flow curve (force f vs velocity v) is non-monotonic, with a minimum at $f = f_{\min}$, there exists a threshold force f_c beyond which the static phase is unstable to system-spanning events. (b) A finite hysteresis is predicted in the thermodynamic limit, such that a system driven quasi-statically through a weak spring displays stick-slip. Thereby, power law distributed avalanches protect the interface from building up a load $f > f_c$ where it is unstable. After the instability, the interface unloads to $f = f_{\min}$ while slipping (see corresponding cycle in panel a with the same colour coding).

¹Such a bimodal distribution for earthquakes on a single fault was argued based on seismic data in [28].

²More precisely, stress levels.

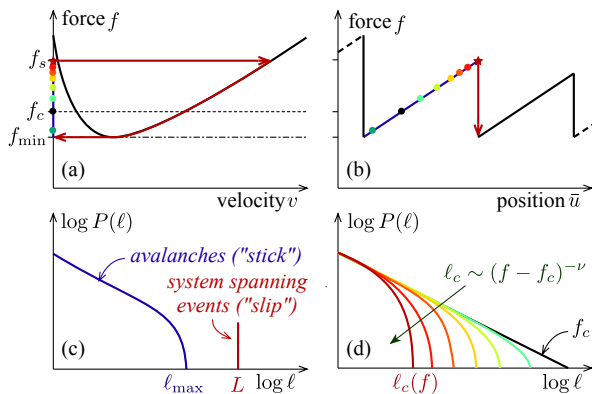


Figure 2. [Sketch] (a-b) In a quasi-statically loaded finite system with disorder, avalanches occur as the force increases. They nucleate slip once their extension $\ell > \ell_c \sim (f - f_c)^{-\nu}$ if $f > f_c$. The force at which nucleation occurs fluctuates, we denote by f_s its means (and study below how the magnitude of hysteresis $\Delta f = f_s - f_c$ depends on L). (c) The corresponding distribution of event extensions, $P(\ell)$, during a quasi-static cycle is bimodal, with avalanches up to a scale $\ell_{\max}(f_s)$, and system-spanning events ($\ell = L$). See Appendix B for numerical evidence of bimodality. (d) To study the properties of avalanches in an infinite system, and to quantify ℓ_c , we trigger avalanches at different forces f . The distribution of their linear extension ℓ is scale free at f_c while at $f > f_c$ avalanches transition to system-spanning events if $\ell > \ell_c$ (system-spanning events are excluded from the shown distributions).

2 Model

Dynamics. We simulate a classical depinning model, however with inertia. In particular, we consider a line in dimension $d = 1$ composed of L particles that have a finite mass, interact elastically with their nearest neighbours, and experience a disordered pinning potential. In our model, each particle (numbered $i = 1, 2, \dots, L$) has a degree of freedom (the position u_i) that follows Newton dynamics. The dynamics then read

$$m\ddot{u}_i = \underbrace{-\partial_u U_i}_{1) \equiv f_i^p} + \underbrace{\Delta u_i}_{2) \equiv f_i^n} + \underbrace{k_f(\bar{u} - u_i)}_{3) \equiv f_i^f} - \underbrace{\eta \dot{u}_i}_{4) \equiv f_i^d} \quad (2)$$

(whereby we use a mass $m = 1$ that is uniform). Here, $\dot{u}_i \equiv \partial_t u_i$ is the particle's velocity and $\ddot{u}_i \equiv \partial_t^2 u_i$ is the particle's acceleration. The restoring force on a particle i is composed of the following terms.

1) Each particle is driven through a potential energy landscape U_i that is piecewise linear elastic with uniform elastic constant $\mu = 1$ and random local barriers, see below.

2) Neighbouring particles interact elastically such that schematically $f_i^n = \Delta u_i$, the Laplacian of u .

We use the fourth order expansion [34, 35] such that in $d = 1$ dimensions, $f_i^n = k_2[u_{i-1} - 2u_i + u_{i+1}] + k_4[(u_{i+1} - u_i)^3 + (u_i - u_{i-1})^3]$ with $k_2 = k_4 = 1$ (see Appendix A.1 for a derivation), so as to avoid an unrealistic roughness exponent $\zeta > 1$ known to occur with overdamped dynamics. Moreover, we assume periodic boundary conditions $u_{L+i} = u_i$ for any i (in particular $u_1 = u_L$). Henceforth, we express length in units of the discretization, such that the system's extension is L .

3) We drive by connecting each particle with a weak spring of stiffness k_f to a “driving frame” whose position \bar{u} is prescribed, see below.

4) Finally, we add a small damping term with uniform viscosity η to each particle. Underdamped dynamics correspond to $\eta^2 < 4\mu m$. We use $\eta = 0.1$ ($\ll 4\mu m \equiv 4$). We study this model numerically by integrating Eq. (2) using the velocity Verlet algorithm, which uses a discrete time step $\Delta t = 0.05$ ³. See Fig. 3 for a schematic of the model for $L = 5$ particles.

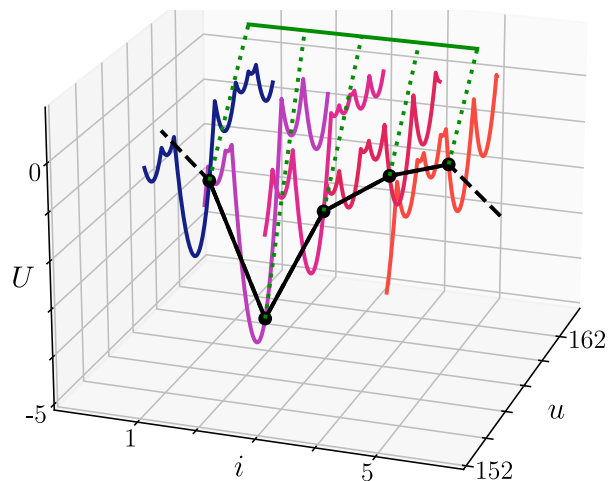


Figure 3. Schematic of our model with equation of motion in Eq. (2) in dimension $d = 1$ for $L = 5$ particles. The potential energy landscape U_i of each particle i is a sequence of parabolic wells with uniform curvature $\mu = 1$ and random widths (that are quenched). In this example, the landscape of each particle is drawn in a different colour. The particle positions u_i are indicated by the black dots. Their elastic interactions are schematically illustrated by black lines (with dashed lines indicating periodicity). The driving frame is indicated by a green line. It is connected to each particle by a weak spring of stiffness k_f illustrated using a dotted green line.

Disorder. For each particle, the potential energy landscape U_i is a sequence of parabolic wells with uniform curvature $\mu = 1$ and random widths (that

³Such that $\Delta t \ll \omega^{-1}$, with $\omega^2 = \mu/m - (\eta/(2m))^2 \approx 1$.

are quenched). The elastic force $f_i^p = \mu(u_i - u_i^{\min})$, with u_i^{\min} the position of the local minimum $u_i^{\min} = (u_i^s + u_i^{s+1})/2$ with $u_i^s = \sum_{y=1}^s u_i^y$ the position of the edge of the well that the particle is currently in. The width of the well, $u_i^{s+1} - u_i^s$, is drawn randomly from a Weibull distribution with shape parameter $k = 2$ ⁴. A crucial quantity is the force needed to fail locally in the forward direction, $x_i \equiv \mu(u_i^{s+1} - u_i)$.

Quasi-static loading. Quasi-static loading corresponds to driving the frame \bar{u} at a zero rate $\partial_t \bar{u} = 0$. In practice, we increase \bar{u} by a small amount and then follow the dynamics until the energy is minimized. This sequence is then repeated until we gathered sufficient statistics (discarding start-up effects). We save significantly on computational time using an event-driven algorithm such that we skip periods with a complete absence of local yielding events, see Appendix A.2 for details. These “events” are the primary object of most of our analysis. We drive using a weak spring of stiffness $k_f = 1/L^2$, whose magnitude matches the stiffness of the modes of wavelength L , so as not to affect the roughness of the line on scales much smaller than L .

Triggering. The quasi-static response provides us with events at different forces f , whereby the response is purely elastic in between events. Since we are interested in the statistics of avalanches at fixed f , we additionally manually trigger avalanches at different f to efficiently gather sufficient statistics. Thereby, we move a randomly selected particle over the first barrier in the forward direction while keeping the position of the driving frame fixed, see Appendix A.3 for details.

3 Nucleation

To test Eq. (1), we first estimate f_c . We then establish a scaling relation for ν . Finally, we test Eq. (1) using measurements of $\ell_c(f)$.

First system-spanning event. We first define f_c as the lowest force at which we observe system-spanning events, if we manually trigger avalanches after a slip event during quasi-static loading. This estimate, done in our largest system, is shown as a dashed line in Fig. 4.

⁴The cumulative distribution of the widths w is $\Phi(w) = 1 - \exp(-(w/w_0)^k)$ with $k = 2$ and $w_0 = 2$. A small offset of 10^{-5} is added such that $w > 0$ (i.e. $\Phi(w \leq 0) = 0$). Note that the average width is $\langle w \rangle \approx 2$, such that the typical yield force is approximately 1 (as we use stiffness $\mu = 1$). Finally, the sequence of wells for each particle i is offset by a random number, such that the local minima around $u_i = 0$ are not correlated.

Flow curve. In practice, the threshold force f_c is predicted to be very close to the minimum of the flow curve f_{\min} [27, 36]. We thus test the approximation $f_c \approx f_{\min}$. To measure the latter, we need to measure the flow curve by driving the interface at a finite rate. However, at small velocities, stick-slip occurs. A classical approach to stabilize the velocity-weakening branch of the flow curve is to drive the system with a stiff spring [25], see also Appendix C. We use $k_f = 0.1$ (as a reference, we note that we recorded the quasi-static response above for $k_f = 1/L^2 \approx 1.5 \times 10^{-8}$). We plot the flow curve in Fig. 4 and find its minimum, confirming that $f_c \approx f_{\min}$. In the Appendix D, we show that our measurement of f_{\min} is robust with changing k_f , as long as the value of k_f and the driving velocity are large enough (since stick-slip occurs otherwise). In that figure, it is also shown that relaxation experiments give the same estimate for f_{\min} .

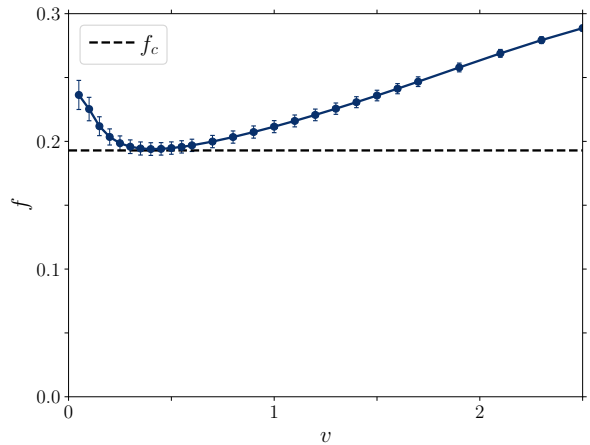


Figure 4. Measured flow curve, showing that the force f at the driving frame is a non-monotonic function of the velocity v . The measurement of the unstable branch (where $\partial_v f < 0$) is possible by driving with a stiff spring. Also indicated: the critical force, f_c , defined the lowest force at which we find system-spanning events.

Scaling relation for ν . To measure the exponent ν , we use the scaling relation relating it to the exponent ζ characterizing the roughness of the interface (i.e. $u \sim \ell^\zeta$):

$$\nu = 1/(2 - \zeta). \quad (3)$$

This is a classical result of the depinning transition, which can be derived based on certain symmetries of the problem. Intuitively, it is simply the statement that on the correlation length $\xi \sim (F - F_c)^{-\nu}$, the fluctuations of elastic force $\delta F \sim \xi^{\zeta-2}$ are of the order of the distance to threshold $F - F_c$. This relation was observed to hold in the presence of inertia [36].

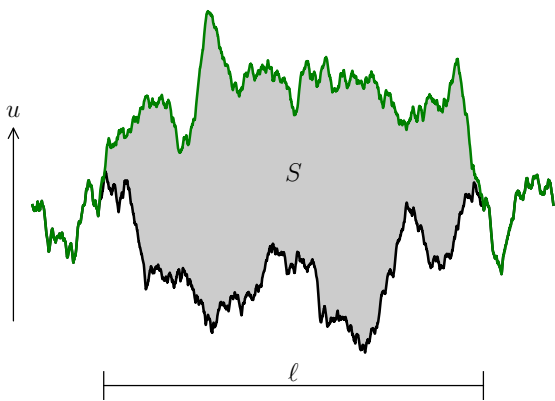


Figure 5. Position of the interface u before (black) and after (green) an avalanche triggered at $f \approx f_c$. The total number of fails, S , is a proxy for the total displacement of the interface (in gray). The number of particles that fail at least once, ℓ (in $d = 1$), is a proxy for the linear extension of the avalanche (annotated).

Scaling relation for ζ . To estimate the roughness exponent ζ , we use the fact that it characterizes how the accumulated total displacement S of an avalanche depends on its spatial extent ℓ , as illustrated in Fig. 5:

$$S \sim \int \delta u dx^d \sim \ell^{d+\zeta}, \quad (4)$$

where we integrate over d dimensions⁵. Practically, we define the size S as the total number of fails, and the extension ℓ as the number of particles that fail at least once (since $d = 1$). Our results are shown in Fig. 6, indicating that $\zeta \approx 0.8$, which corresponds to $\nu \approx 0.83$.

Nucleation radius. We measure the nucleation radius $\ell_c(f)$ using the distribution of events triggered at different f . We consider only the statistics of avalanches, i.e. we discard the mode in the distribution corresponding to system-spanning event with $\ell = L$. $\ell_c(f)$ corresponds to the cut-off of the distribution of avalanche extension, which we estimate as is often done as $\ell_c = \langle \ell^3 \rangle / \langle \ell^2 \rangle$, where the average is made on all avalanches. Results are shown in the inset of Fig. 7.

To test Eq. (1), we employ a finite size collapse in Fig. 7 whereby we find $\nu \simeq 0.9$, in rather good agreement with the measurement of the avalanche fractal exponent in Fig. 6, which led to $\nu \approx 0.83$, using the scaling relation Eq. (3). Supporting measurements based on a different protocol to extract ℓ_c are presented in Appendix E. Thus, the fact that

⁵Note that this exponent is commonly named the fractal dimension d_f (i.e. $S \sim \ell^{d_f}$ with $d_f = d + \zeta$).

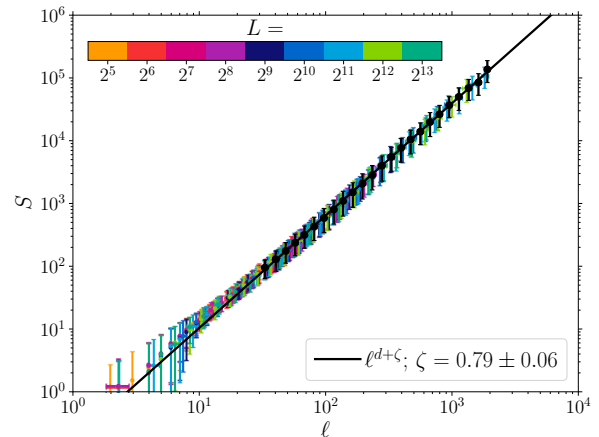


Figure 6. Measurement of the fractal dimension at $f \approx f_c$: the size S of avalanches as a function of their extension ℓ , and a fit of the scaling relation of Eq. (4) $S \sim \ell^{d+\zeta}$ as a solid black line (fit on the binned data for all avalanches for all considered system sizes, shown using black markers). The coloured markers correspond to a binning of individual (manually triggered) avalanches for different L . Note that we only show avalanches and remove system-spanning events (which at f_c is only a small fraction of the events).

nucleation is controlled by a critical point, despite that the flowing regime displays a first order transition, appears to hold in short-range depinning as well.

4 Effect of system size on the magnitude of the hysteresis cycle

From our viewpoint, there exists a tiny hysteresis in the thermodynamic limit $f_c - f_{\min}$, which, however, is too small for us to resolve. Yet, the observed hysteresis (the amplitude of the stick-slip cycle) is actually very large in our numerics, which we now explain.

Theoretical arguments. We obtain a prediction for the amplitude of the stick-slip cycle $\Delta F(L)$ if we combine (i) the rate at which avalanches are nucleated, and (ii) the statistics of avalanches, with the above picture of nucleation.

(i) Armouring of the interface. Significant mechanical noise is generated during a system spanning event. This has the consequence that it is unlikely to find regions that are about to fail after such an event (as they would have failed during the event). This is reflected in the additional force x needed to trigger avalanches locally. It was argued that such effect should lead to a density that follows [29, 30] $P(x) \sim x^{\theta'}$. As a result, the number of avalanches, n_a , triggered as the force is increased

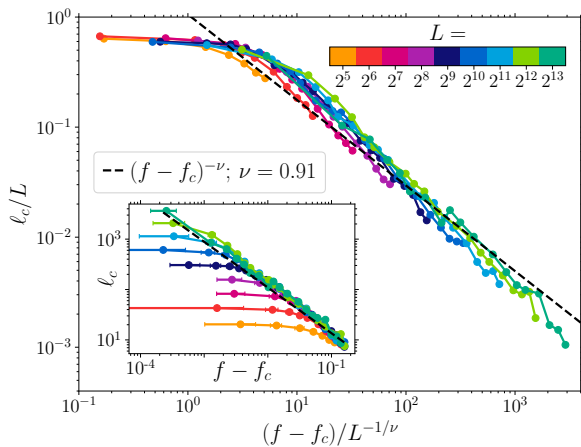


Figure 7. Characterization of the nucleation length ℓ_c beyond which avalanches are unstable, as a function of force f . We define ℓ_c as the upper cut-off of the distribution of avalanche’s linear extension: $\ell_c = \langle \ell^3 \rangle / \langle \ell^2 \rangle$ (with $\langle \dots \rangle$ the average over events that are not system-spanning, i.e. $\ell < L$). The best collapse is obtained for $\nu \approx 0.9$.

from f_{\min} to $f_{\min} + \Delta f \approx f_c + \Delta f$ follows:

$$n_a \sim L \int_0^{\Delta f} P(x) dx \sim L(\Delta f)^{\theta'+1}. \quad (5)$$

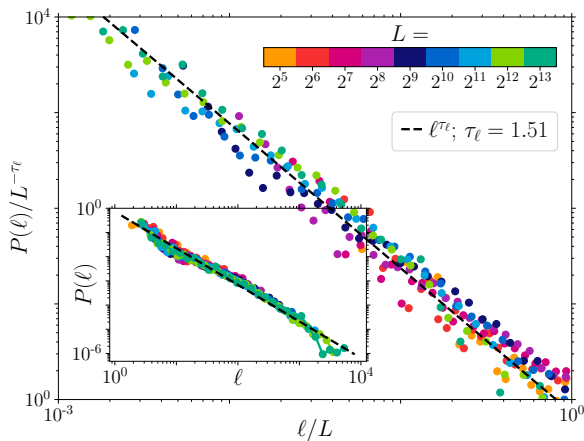


Figure 8. Distribution of avalanche extension, $P(\ell)$, at $f \approx f_c$. The exponent τ_ℓ is shown using a dashed black line. The inset shows $P(\ell)$ while the main panel shows the finite size collapse with that value of τ_ℓ .

(ii) Avalanche statistics. Near f_c , the distribution of avalanche extension is power law: $P(\ell) \sim \ell^{-\tau_\ell}$. To measure τ_ℓ , we measure the distribution of the avalanche extension, $P(\ell)$, at $f \approx f_c$ as shown in Fig. 8. We obtain $\tau_\ell \approx 1.5$.

Maximal extension of avalanches and nucleation. Given n_a avalanches, if ℓ_{\max} denotes the

typical extension of the largest avalanche, extreme value statistics [37] implies that:

$$n_a \int_{\ell_{\max}}^{\infty} P(\ell) d\ell \sim 1 \quad (6)$$

leading to:

$$\ell_{\max} \sim n_a^{-1/(1-\tau_\ell)}. \quad (7)$$

Nucleation will occur when ℓ_{\max} reaches the nucleation length $\ell_c \sim \Delta f^{-\nu}$. This situation corresponds to the intersection of the gold and red lines in Fig. 9, which illustrates the present argument.

Stick-slip amplitude. Using Eqs. (5) and (7) leads to the main result:

$$\Delta f \sim L^{-1/(\theta'+1-\nu(1-\tau_\ell))}. \quad (8)$$

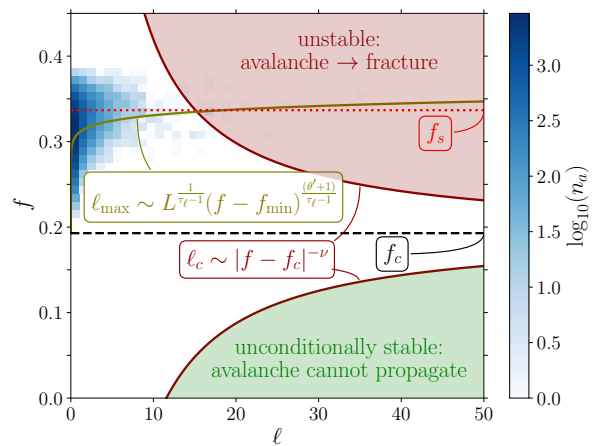


Figure 9. Spontaneous nucleation of slip during the stick-slip cycle in a finite system. Once stopped at f_{\min} after a slip event, the system is “armoured” such that there are very few regions close to yielding. Due to this effect, the scale ℓ_{\max} of the largest avalanche grows very slowly with increasing force (gold curve). When this curve hits the nucleation size ℓ_c (red line), nucleation occurs and a system spanning event is triggered. In blue: the number of avalanches with a certain extension for avalanches triggered naturally during quasi-static loading, as indicated by the colour bar. The lines corresponding to the predictions of ℓ_{\max} (gold) and ℓ_c (red) are based on measured exponents, with arbitrary prefactors. The green region is indicated for completeness, as the region where avalanches cannot propagate, see [1].

Empirical tests. To test Eq. (8), we first measure $\theta' \simeq 6.4$ in Fig. 10 by comparing the total number of collective events⁶ upon increasing the driving force by Δf after a system-spanning event.

⁶Collective events are defined as events involving at least two rearrangements, see Appendix F and [29] for a discussion.

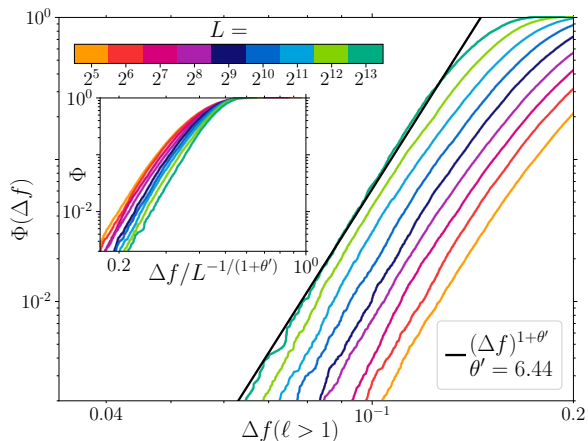


Figure 10. Cumulative number of avalanches, Φ , upon increasing the driving force by Δf after a system-spanning event, from which the exponent θ' is obtained.

Finally, we measure the magnitude of the hysteresis cycle $\Delta f(L) = f_s - f_{\min}$, where f_s is the average force right before a spanning event (in red) and f_{\min} the average force right after it (in blue). The scaling prediction of Eq. (8) is tested in inset, and shows an excellent agreement with our predictions.

5 Conclusion

We have tested a theory for the short-range depinning transition when velocity weakening is present, as can occur e.g. for weak damping when inertia plays a large role. This theory builds on the continuous rate-and-state framework to describe homogeneous frictional interfaces, and treat disorder perturbatively [1]. We have confirmed in the case of a pinned elastic line that in the presence of velocity weakening, the depinning transition has a surprising mixed behaviour. Specifically, the flowing phase has properties of a first order phase transition: the flow curve is non-monotonic, leading to a finite amount of hysteresis. When nucleation occurs, it generates flow at a finite speed. Yet, the avalanche-type response in the solid phase is controlled by a continuous critical point, predicted to be just above the minimum of the flow curve. Scale free avalanches are present, which control the nucleation process. The latter leads to immense finite size effects on the magnitude of hysteresis. This phenomenology is reminiscent of faults, paradoxically known to display power-law distributed avalanches as well as fault-spanning earthquakes that can be suddenly triggered, reminiscent of a nucleation process.

Note that the present model could be used to study larger damping, for which velocity-weakening may disappear and [scenario B](#) discussed in the in-

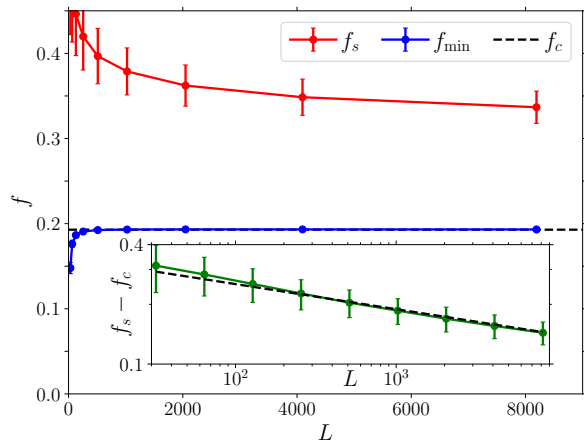


Figure 11. Main panel: Finite size scaling of the force just before system-spanning events (f_s in red) and just after system-spanning events (f_{\min} in blue). The markers correspond to the means and the error bars to the standard deviation. Inset: finite size scaling of the stick-slip amplitude $f_s - f_c$ with f_c the smallest force at which a system-spanning event was found to occur in any of our finite systems (also shown in the main panel using a dashed black line). The dotted line corresponds to our prediction in Eq. (8), with exponents taken from Figs. 7, 8 and 10.

roduction could apply. It would also allow one to study how exponents cross-over between an overdamped and underdamped regime [14, 20, 21].

Finally, another interesting question concerns the applicability of the proposed scenario to other systems. A bimodal distribution of avalanches is also observed in amorphous solids under stress when inertia is important [38]. A pseudo-gap in the distribution of local yield stress must be present in these systems even in the overdamped limit [32], but it is enhanced by inertia that increases its associated exponent θ [38]. It remains to be seen if the minimum of the flow curve controls the nucleation of rupture in that case as well.

Acknowledgements

Damien Ribière is thanked for derivations concerning the stabilization of the velocity weakening instability by a stiff driving spring. Alberto Rosso is thanked for discussions. T.G. acknowledges support from the Swiss National Science Foundation (SNSF) by the SNSF Ambizione Grant PZ00P2_185843. M.W. acknowledges support from the Simons Foundation Grant (No. 454953 Matthieu Wyart).

A Model

A.1 Interactions

Following [34], we consider elastic interactions with a potential energy density that we expand to the fourth order:

$$E(\mathbf{x}) = \frac{1}{2}k_2(\varepsilon(\mathbf{x}))^2 + \frac{1}{12}k_4(\varepsilon(\mathbf{x}))^4, \quad (\text{A1})$$

with \mathbf{x} the spatial coordinate along the interface, k_2 and k_4 stiffnesses, and the gradient of the position $\varepsilon = ||\partial_{\mathbf{x}}u||$. The resulting force $f^n(\mathbf{x}) = \text{div} \partial_{\varepsilon}E(\mathbf{x})$. In $d = 1$ the geometry corresponds to an elastic line, for which

$$f^n(x) = \frac{\partial^2 u}{\partial x^2} \Big|_x \left(k_2 + k_4 \left(\frac{\partial u}{\partial x} \Big|_x \right)^2 \right), \quad (\text{A2})$$

which we discretize as [35]:

$$f_i^n = k_2[u_{i-1} - 2u_i + u_{i+1}] + k_4[(u_{i+1} - u_i)^3 + (u_i - u_{i-1})^3]. \quad (\text{A3})$$

We use $k_2 = k_4 = 1$ ⁷. Note that we have expressed x in units of the ‘discretization’ $h = 1$, such that the length of the line is L . Finally, we assume periodic boundary conditions such that $u_1 = u_L$ ⁸.

A.2 Event-driven quasi-static loading

Since the system is linear as long a no particle fails, we know the particle positions u_i satisfying the mechanical equilibrium for any driving frame position \bar{u} that matches the condition that all particles stay in their current potential well. This allows the following protocol. In alternation, we set $\bar{u}(t + \Delta t) = \bar{u}(t) + \Delta u(1 + \mu/k_f)$ and $u_i(t + \Delta t) = u_i(t) + \Delta u$ for all i , as follows. First, we perform a fully elastic step whereby the displacement Δu is chosen such that the particle closest to failing in the direction of driving ends at the verge of failing. In particular, $\Delta u = (\min(x_i)/\mu - \epsilon/2)_+$ (with the Macaulay brackets $(\dots)_+$ indicating that the term is zero if the argument is negative, and $\epsilon = 10^{-3}$). Since, by definition, no particle fails during this step, the system stays in mechanical equilibrium. Second, we apply a ‘kick’ and set $\Delta u = \epsilon$ followed by energy minimization using the dynamics in Eq. (2). Whatever happens during this step we refer to as an ‘event’, and they are the primary object of most of our analysis.

⁷For overdamped dynamics, this model has as known limitation in $d = 1$ that linear elasticity ($k_4 = 0$) results in an unphysical roughness $\zeta_{\infty} > 1$, while $\zeta_{\infty} = 0.63$ if $k_4 > 0$ [34, 35]. This is unimportant for our scaling prediction. However, we stick to the physical case and choose $k_2 = k_4 = 1$ in $d = 1$.

⁸In fact, $u_{L+i} = u_i$ for any i .

We collect the following number of events during quasi-static loading, for a system with L particles: $L = 2^5$: 357818, $L = 2^6$: 199964, $L = 2^7$: 199953, $L = 2^8$: 199934, $L = 2^9$: 84416, $L = 2^{10}$: 64224, $L = 2^{11}$: 72025, $L = 2^{12}$: 89594, $L = 2^{13}$: 32257.

A.3 Triggering

For different f and starting from each system-spanning event, we select the state with the highest $f_q < f$ acquired by normal quasi-static loading (hence the subscript q). We elastically load that state up to f (by advancing the driving frame by $\Delta\bar{u} = (f - f_q)/k_f$, and moving u_i accordingly to maintain mechanical equilibrium, see Appendix A.2). Then, while keeping the boundary condition \bar{u} fixed, we move a particle over the first barrier in the forward direction such that $u_i = u_i^{s+1} + \epsilon/2$ for a randomly selected⁹ i and minimize energy. In practice, starting from each system-spanning event, we load with different Δf and then bin on f .

B Bimodal distribution

During the stick-slip cycle, we observe two populations of collective events: avalanches and system-spanning events. Avalanches are the largest fraction of these collective events. These are events in which one or more, *but not all*, particles fail at least once, such that $\ell < L$. We quantify this observation in Fig. A1. In the main panel, the distribution of the event sizes $P(S)$ for different system sizes L shown using different colours. Thereby, S represents the total displacement of the line, and is defined as the total number of fails during an event. We clearly observe two populations of events: *avalanches* on the left and side, and *system-spanning* events on the right-hand side. Only for small systems, these two modes of the distribution merge into a single one, see e.g. [39].

The system-spanning events are ‘slip’ events during which the system accumulates macroscopic slip, while sub-extensive avalanches occur during the ‘stick’ phase of the stick-slip cycle. The fraction of events that are avalanches is shown in the inset as a function of system size L . As observed, this fraction approaches one for large L .

⁹For a fraction of particles, the particle’s failure will not trigger an avalanche. To save on computational time, we rapidly assess, using entirely heuristic measures, if that is the case. If so, we select another particle. This does not result in any quantitative data about which particles are more likely to trigger an avalanche, since, without energy minimization, we cannot ensure if the particle truly did not trigger an avalanche. Precisely that energy minimization we chose to avoid by using heuristic rules, to save on computational time.

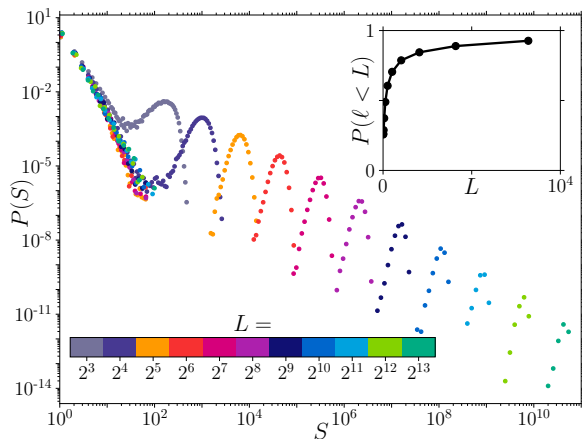


Figure A1. Distribution of the event sizes S of any event (“avalanche” or “system-spanning”) during quasi-static loading, for different system sizes as indicated using different colours (see values of the system size L in the colour bar). *Avalanches*, cut-off at a small radius, constitute the majority of events (inset: fraction of events that are avalanches as a function of system size L). *System-spanning*, or “slip”, events span the entire system, and constitute the right-hand side peak whose position increases with the system size L .

C Stability of rate-and-state friction

Consider a single particle with mass m that is driven by a spring of stiffness k_f . Furthermore, it is subjected to velocity weakening rate-and-state friction. In such a model, the friction force

$$f_p = f_0 + a \ln(v_i/v_0) + b \ln(v_0\chi/D_c). \quad (\text{A4})$$

Here, f_0 , a , and b are parameters with the units of force here; v_0 sets the units of velocity; χ is the age of the interface; and D_c is the sliding distance needed to rejuvenate the interface. We complement this law with a simple ageing law

$$\dot{\chi} = 1 - v_i\chi/D_c. \quad (\text{A5})$$

For this law, the steady state age, after rejuvenation has completed, corresponds to

$$\chi_\infty = D_c/v_i. \quad (\text{A6})$$

We stabilize this rheology by adding a viscous term ηv_i .

In the steady state, the resulting rheology is non-monotonic, with a minimum at $v_c = (b-a)/\eta$. The unstable branch, where $\partial_v f < 0$, corresponds to $v < v_c$. The stable branch, where $\partial_v f > 0$, corresponds to $v > v_c$.

Supposing that the particle is in a steady state in mechanical equilibrium (such that the particle

exactly follows the drive as $v_i = v$), force balance corresponds to

$$\underbrace{f_0 + a \ln\left(\frac{v}{v_0}\right) + b \ln\left(\frac{v_0\chi_\infty}{D_c}\right)}_{\text{rate-and-state}} + \underbrace{\eta v}_{\text{heat}} = \underbrace{k_f(vt - u_i)}_{\text{drive}}. \quad (\text{A7})$$

We will now consider the effect of a small perturbation $v + \delta v$, $\chi_\infty + \delta\chi$, and $u_i + \delta u$. This results in

$$\delta v(a/v + \eta) + \delta\chi b/\chi_\infty = -k_f\delta u. \quad (\text{A8})$$

Applying the same perturbation to the ageing law (still around the steady state) results in

$$\delta\dot{\chi} = -\delta v/v - \delta\chi/\chi_\infty. \quad (\text{A9})$$

Combining it with the time derivative of Eq. (A8) results in

$$\begin{cases} \delta\dot{v}(a/v + \eta) + \delta\dot{\chi}b/\chi_\infty = -k_f\delta v \\ \delta\dot{\chi} = -\delta v/v - \delta\chi/\chi_\infty \end{cases} \quad (\text{A10})$$

Let us make the ansatz $\delta v = v_0 e^{\lambda t}$ and $\delta\chi = \chi_0 e^{\lambda t}$ (with λ a complex number) and search for solutions. After some algebra, we find

$$\lambda^2 \left(\frac{a}{v} + \eta\right) + \lambda \left(\frac{a-b+\eta v}{D_c} + k_f\right) + \frac{k_f v}{D_c} = 0 \quad (\text{A11})$$

Now, the perturbation will grow exponentially in time if $\text{Re}(\lambda) > 0$, while they will decay exponentially if $\text{Re}(\lambda) < 0$. The critical case therefore corresponds to $\text{Re}(\lambda_c) = 0$, such that $\lambda_c = i\text{Im}(\lambda)$. This implies that $-\text{Im}(\lambda_c)(a/v + \eta) + k_f v/D_c = 0$ and $\text{Im}(\lambda_c)((a-b+\eta v)/D_c + k_f) = 0$. From the latter, it follows that the critical stiffness is

$$k_f = (b-a-\eta v)/D_c \equiv k_c. \quad (\text{A12})$$

If $k_f < k_c$, a perturbation will grow exponentially, and the system is unstable. If $k_f > k_c$, a perturbation will decay exponentially, and the system is stable. In this case, the particle will not show stick-slip even if driven at a rate $v < v_c$.

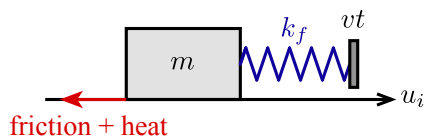


Figure A2. Simple model of a single particle subject to a rate-and-state friction force and heat radiation, and driving at a velocity v by a weak spring of stiffness k_f .

D Measuring f_{\min}

Driven interface stabilised by a stiff spring.

We measure the rheology of our model by driving the system at a finite rate v ¹⁰ and measuring the average force experienced by the driving frame f . We consider only the steady state response. Any transient start-up effects or intermittent response is discarded. We consider our largest system $L = 2^{13}$ and measure the rheology for different stiffnesses k_f (as a reference, we note that we recorded the quasi-static response above for $k_f = 1/L^2 \approx 1.5 \times 10^{-8}$). The results are shown in Fig. A3. The different blue curves correspond to different stiffnesses k_f (see colour bar). The non-monotonic rheology is evidenced when driving with a stiff spring. However, the rheology is an interplay between the response of the interface and the driving spring, as clearly observed. We do not understand the details of this interplay, and from Fig. A3 it seems non-trivial, as the order of the curves is not monotonic in k_f . Objectively extracting f_{\min} (and v_{\min}) from this data is therefore currently not possible, and future work is urged.

Relaxation. We propose an alternative protocol to measure the rheology. We measure the relaxation during a system-spanning slip event during quasi-static loading (again using the low, reference, k_f). In particular, we measure the force experienced by the driving frame, f , as a function of the average velocity of the interface, v . The result is shown in Fig. A3 using a green curve. This protocol cannot acquire the unstable branch of the rheology, but it does allow measuring the stable branch. It is tempting to speculate that it does so until $v = v_c$. If that is the case, we find a good agreement between the minimum of the rheology, f_{\min} , and the definition of f_c that we used above.

E Alternative measurement of ℓ_c

In the main text, we defined $\ell_c = \langle \ell^3 \rangle / \langle \ell^2 \rangle$. Here we use an alternative protocol where we fit an exponentially cut-off power law to the cumulative distribution $\Phi(\ell) \sim \ell^{1-\tau_\ell} \exp(-\ell/\ell_c)$. The result in Fig. A4 is indeed also consistent with our prediction in Eqs. (1) and (3).

F Armouring

Distribution of local yield stress $P(x)$. The distribution of local yield stress after system-spanning events contains information about the number of plastic events that can be triggered upon

¹⁰At every time step we move the driving frame $\bar{u}(t+\Delta t) = \bar{u}(t) + v\Delta t$.

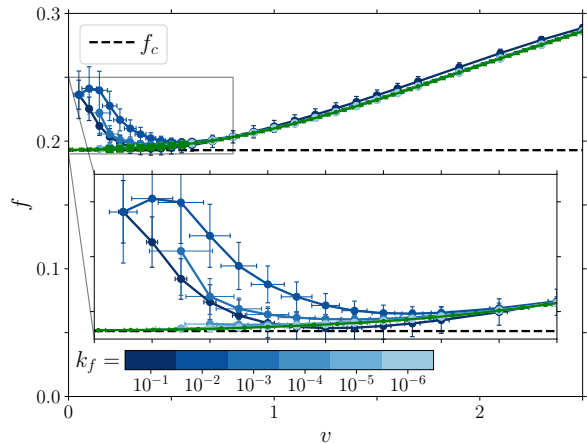


Figure A3. For the largest system. Green curve: relaxation measurement: the force and velocity are measured during a system-spanning event. The shown data is the average force per bin of velocity. The large square green markers correspond to measurements of the force if the system is driven at a constant, finite rate. Measurements in which the system intermittently stops are discarded. The same type of measurement is shown for different driving stiffnesses in blue (see colour bar).

increasing the load. We measure x_i as the additional force needed to fail a particle i in the forward direction. The density $P(x)$ is consistent with a pseudo-gap distribution

$$P(x) \sim x^\theta, \quad (\text{A13})$$

see lower-left inset in Fig. A5. However, extracting θ from the noisy data is difficult. The proper measurement of the exponent is therefore to perform extreme value statistics using finite size scaling. Once again, we employ the result of [37] to argue that

$$L \int_0^{x_{\min}} P(x) dx \sim 1, \quad (\text{A14})$$

(with L the number of particles). Assuming the pseudo-gap distribution of Eq. (A13), we find that $x_{\min} \sim L^{-1/(1+\theta)}$. Our data is consistent with this result with $\theta = 3.2$ as shown in the main panel of Fig. A5. This result is not far from our earlier result of $\theta = 3.7$ [29] in our model based on long-range elasticity. Furthermore, this value is of the same order as a prediction based on a single particle model [30], see [40] for other results in a single particle model.

Only a vanishing fraction of plastic events can trigger avalanches. Our main result depends on θ' , which is based on the actual number of avalanches (in which at least two particles fail) upon increasing the load by Δf after a system-spanning event. Interestingly, we find that $\theta < \theta'$, cf. Figs. 10

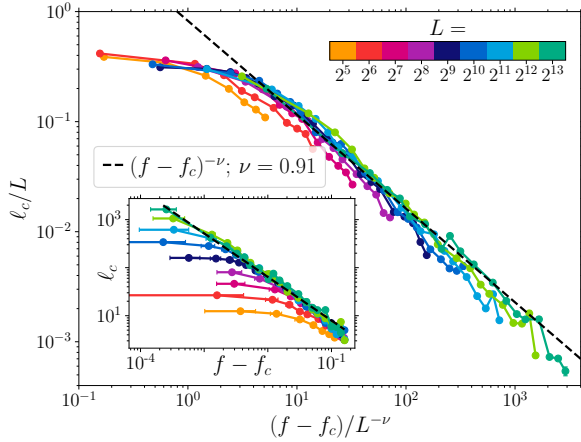


Figure A4. Complementary to Fig. 7 we measure ℓ_c by fitting an exponential cut-off to the cumulative distribution of the linear extension of avalanches (see text), and verify that our data is consistent with the prediction in Eqs. (1) and (3).

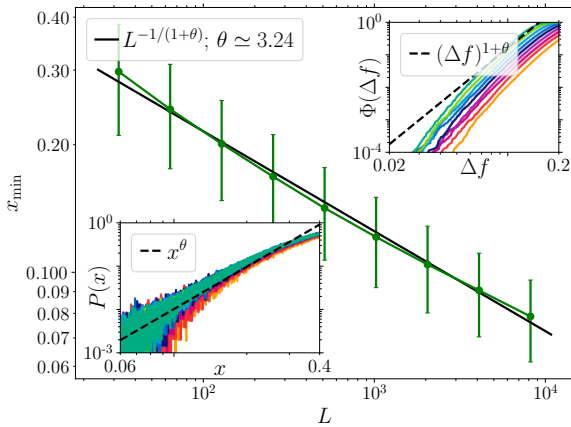


Figure A5. Characterization of (force) barriers after system-spanning events. The force needed to trigger failure locally $x_i \equiv \mu(u_i^Y - u_i)$ with u_i^Y the position of the edge of the local potential in the direction of triggering. Plotted is x_{\min} as a function of the number of particles L , which allows fitting the exponent θ of $P(x) \sim x^\theta$ as indicated (see also main text). x_{\min} is taken as the mean of the minimum of x after L system-spanning events, see Appendix A.2. Lower-left inset: $P(x)$ for different system sizes. Upper-right inset: cumulative number of events upon increasing the driving force by Δf after a system-spanning event. In both cases, the black line corresponds to the θ fitted in the main plot.

and A5. We thus find, as for long-range elasticity [29], that not all failures trigger an avalanche.

References

- [1] T. W. J. de Geus and M. Wyart. Scaling theory for the statistics of slip at frictional interfaces. *Phys. Rev. E*, 106(6):065001, 2022. doi: [10.1103/PhysRevE.106.065001](https://doi.org/10.1103/PhysRevE.106.065001). arXiv: [2204.02795](https://arxiv.org/abs/2204.02795).
- [2] E. Bouchaud. Scaling properties of cracks. *J. Phys. Condens. Matter*, 9(21):4319–4344, 1997. doi: [10.1088/0953-8984/9/21/002](https://doi.org/10.1088/0953-8984/9/21/002).
- [3] C. H. Scholz. Earthquakes and friction laws. *Nature*, 391(6662):37–42, 1998. doi: [10.1038/34097](https://doi.org/10.1038/34097).
- [4] K. A. Dahmen and J. P. Sethna. Hysteresis, avalanches, and disorder-induced critical scaling: A renormalization-group approach. *Phys. Rev. B*, 53(22):14872–14905, 1996. doi: [10.1103/PhysRevB.53.14872](https://doi.org/10.1103/PhysRevB.53.14872).
- [5] S. Zapperi, P. Cizeau, G. Durin, and H. E. Stanley. Dynamics of a ferromagnetic domain wall: Avalanches, depinning transition, and the Barkhausen effect. *Phys. Rev. B*, 58(10):6353–6366, 1998. doi: [10.1103/PhysRevB.58.6353](https://doi.org/10.1103/PhysRevB.58.6353).
- [6] O. Narayan and D. S. Fisher. Critical behavior of sliding charge-density waves in 4- ϵ dimensions. *Phys. Rev. B*, 46(18):11520–11549, 1992. doi: [10.1103/PhysRevB.46.11520](https://doi.org/10.1103/PhysRevB.46.11520).
- [7] G. Blatter, M. V. Feigel'man, V. B. Geshkenbein, A. I. Larkin, and V. M. Vinokur. Vortices in high-temperature superconductors. *Rev. Mod. Phys.*, 66(4):1125–1388, 1994. doi: [10.1103/RevModPhys.66.1125](https://doi.org/10.1103/RevModPhys.66.1125).
- [8] M. Kardar. Nonequilibrium dynamics of interfaces and lines. *Phys. Rep.*, 301(1–3):85–112, 1998. doi: [10.1016/S0370-1573\(98\)00007-6](https://doi.org/10.1016/S0370-1573(98)00007-6).
- [9] D. S. Fisher. Collective transport in random media: From superconductors to earthquakes. *Phys. Rep.*, 301(1–3):113–150, 1998. doi: [10.1016/S0370-1573\(98\)00008-8](https://doi.org/10.1016/S0370-1573(98)00008-8).
- [10] O. Narayan and D. S. Fisher. Threshold critical dynamics of driven interfaces in random media. *Phys. Rev. B*, 48(10):7030–7042, 1993. doi: [10.1103/PhysRevB.48.7030](https://doi.org/10.1103/PhysRevB.48.7030).
- [11] T. Baumberger and C. Caroli. Solid friction from stick-slip down to pinning and aging. *Adv. Phys.*, 55(3–4):279–348, 2006. doi: [10.1080/00018730600732186](https://doi.org/10.1080/00018730600732186).
- [12] J. K. Trømborg, H. A. Sveinsson, K. Thøgersen, J. Scheibert, and A. Malthe-Sørenssen. Speed of fast and slow rupture fronts along frictional interfaces. *Phys. Rev. E*, 92(1):012408, 2015. doi: [10.1103/PhysRevE.92.012408](https://doi.org/10.1103/PhysRevE.92.012408). arXiv: [1501.03110](https://arxiv.org/abs/1501.03110).
- [13] S. Ramanathan, D. Ertas, and D. S. Fisher. Quasistatic Crack Propagation in Heterogeneous Media. *Phys. Rev. Lett.*, 79(5):873–876, 1997. doi: [10.1103/PhysRevLett.79.873](https://doi.org/10.1103/PhysRevLett.79.873).
- [14] D. Ertas and M. Kardar. Dynamic roughening of directed lines. *Phys. Rev. Lett.*, 69(6):929–932, 1992. doi: [10.1103/PhysRevLett.69.929](https://doi.org/10.1103/PhysRevLett.69.929).
- [15] A. Prevost, E. Rolley, and C. Guthmann. Dynamics of a helium-4 meniscus on a strongly disordered cesium substrate. *Phys. Rev. B*, 65(6):064517, 2002. doi: [10.1103/PhysRevB.65.064517](https://doi.org/10.1103/PhysRevB.65.064517).
- [16] M. C. Marchetti. Models of plastic depinning of driven disordered systems. *Pramana - J Phys*, 64(6):1097–1107, 2005. doi: [10.1007/BF02704171](https://doi.org/10.1007/BF02704171).
- [17] A. Nicolas, J. L. Barrat, and J. Rottler. Effects of Inertia on the Steady-Shear Rheology of Disordered Solids. *Phys. Rev. Lett.*, 116(5):058303, 2016. doi: [10.1103/PhysRevLett.116.058303](https://doi.org/10.1103/PhysRevLett.116.058303). arXiv: [1508.06067](https://arxiv.org/abs/1508.06067).
- [18] K. Karimi and J. L. Barrat. Role of inertia in the rheology of amorphous systems: A finite-element-based elastoplastic model. *Phys. Rev. E*, 93(2):022904, 2016. doi: [10.1103/PhysRevE.93.022904](https://doi.org/10.1103/PhysRevE.93.022904).
- [19] D. S. Fisher, K. A. Dahmen, S. Ramanathan, and Y. Ben-Zion. Statistics of Earthquakes in Simple Models of Heterogeneous Faults. *Phys. Rev. Lett.*, 78(25):4885–4888, 1997. doi: [10.1103/PhysRevLett.78.4885](https://doi.org/10.1103/PhysRevLett.78.4885).

- [20] K. M. Salerno, C. E. Maloney, and M. O. Robbins. Avalanches in Strained Amorphous Solids: Does Inertia Destroy Critical Behavior? *Phys. Rev. Lett.*, 109(10):105703, 2012. doi: [10.1103/PhysRevLett.109.105703](https://doi.org/10.1103/PhysRevLett.109.105703). arXiv: [1204.5965](https://arxiv.org/abs/1204.5965).
- [21] K. M. Salerno and M. O. Robbins. Effect of inertia on sheared disordered solids: Critical scaling of avalanches in two and three dimensions. *Phys. Rev. E*, 88(6):062206, 2013. doi: [10.1103/PhysRevE.88.062206](https://doi.org/10.1103/PhysRevE.88.062206). arXiv: [1309.1872](https://arxiv.org/abs/1309.1872).
- [22] J. M. Schwarz and D. S. Fisher. Depinning with dynamic stress overshoots: A hybrid of critical and pseudohysteretic behavior. *Phys. Rev. E*, 67(2):021603, 2003. doi: [10.1103/PhysRevE.67.021603](https://doi.org/10.1103/PhysRevE.67.021603).
- [23] R. Maimon and J. M. Schwarz. Continuous Depinning Transition with an Unusual Hysteresis Effect. *Phys. Rev. Lett.*, 92(25):255502, 2004. doi: [10.1103/PhysRevLett.92.255502](https://doi.org/10.1103/PhysRevLett.92.255502).
- [24] J. H. Dieterich. Modeling of rock friction: 1. Experimental results and constitutive equations. *J. Geophys. Res.*, 84(B5):2161, 1979. doi: [10.1029/JB084iB05p02161](https://doi.org/10.1029/JB084iB05p02161).
- [25] J. R. Rice and A. L. Ruina. Stability of Steady Frictional Slipping. *J. Appl. Mech.*, 50(2):343–349, 1983. doi: [10.1115/1.3167042](https://doi.org/10.1115/1.3167042).
- [26] G. Zheng and J. R. Rice. Conditions under which velocity-weakening friction allows a self-healing versus a cracklike mode of rupture. *Bull. Seismol. Soc. Am.*, 88(6):1466–1483, 1998.
- [27] E. A. Brener, M. Aldam, F. Barras, J. F. Molinari, and E. Bouchbinder. Unstable Slip Pulses and Earthquake Nucleation as a Nonequilibrium First-Order Phase Transition. *Phys. Rev. Lett.*, 121(23):234302, 2018. doi: [10.1103/PhysRevLett.121.234302](https://doi.org/10.1103/PhysRevLett.121.234302). arXiv: [1807.06890](https://arxiv.org/abs/1807.06890).
- [28] S. G. Wesnousky. The Gutenberg-Richter or characteristic earthquake distribution, which is it? *Bull. Seismol. Soc. Am.*, 84(6):1940–1959, 1994. doi: [10.1785/BSSA0840061940](https://doi.org/10.1785/BSSA0840061940).
- [29] T. W. J. de Geus, M. Popović, W. Ji, A. Rosso, and M. Wyart. How collective asperity detachments nucleate slip at frictional interfaces. *Proc. Natl. Acad. Sci.*, 116(48):23977–23983, 2019. doi: [10.1073/pnas.1906551116](https://doi.org/10.1073/pnas.1906551116). arXiv: [1904.07635](https://arxiv.org/abs/1904.07635).
- [30] E. El Sergany, M. Wyart, and T. W. J. De Geus. Armouring of a Frictional Interface by Mechanical Noise. *J Stat Phys*, 191(10):134, 2024. doi: [10.1007/s10955-024-03339-z](https://doi.org/10.1007/s10955-024-03339-z). arXiv: [2301.13802](https://arxiv.org/abs/2301.13802).
- [31] M. Müller and M. Wyart. Marginal Stability in Structural, Spin, and Electron Glasses. *Annu. Rev. Condens. Matter Phys.*, 6(1):177–200, 2015. doi: [10.1146/annurev-conmatphys-031214-014614](https://doi.org/10.1146/annurev-conmatphys-031214-014614).
- [32] J. Lin, E. Lerner, A. Rosso, and M. Wyart. Scaling description of the yielding transition in soft amorphous solids at zero temperature. *Proc. Natl. Acad. Sci.*, 111(40):14382–14387, 2014. doi: [10.1073/pnas.1406391111](https://doi.org/10.1073/pnas.1406391111). arXiv: [1403.6735](https://arxiv.org/abs/1403.6735).
- [33] E. A. Jagla. Strain localization driven by structural relaxation in sheared amorphous solids. *Phys. Rev. E*, 76(4):046119, 2007. doi: [10.1103/PhysRevE.76.046119](https://doi.org/10.1103/PhysRevE.76.046119).
- [34] A. Rosso and W. Krauth. Origin of the Roughness Exponent in Elastic Strings at the Depinning Threshold. *Phys. Rev. Lett.*, 87(18):187002, 2001. doi: [10.1103/PhysRevLett.87.187002](https://doi.org/10.1103/PhysRevLett.87.187002).
- [35] A. Rosso. *Dépiégeage de variétés élastiques en milieu aléatoire*. PhD thesis, Université Paris IV, 2002. URL <https://theses.hal.science/tel-00002097>.
- [36] T. W. J. de Geus. E-L-M, simple principles to keep data and code alive. *Preprint*, 2023. doi: [10.31222/osf.io/8tzb9](https://doi.org/10.31222/osf.io/8tzb9).
- [37] J. P. Bouchaud and A. Georges. Anomalous diffusion in disordered media: Statistical mechanisms, models and physical applications. *Phys. Rep.*, 195(4–5):127–293, 1990. doi: [10.1016/0370-1573\(90\)90099-N](https://doi.org/10.1016/0370-1573(90)90099-N).
- [38] K. Karimi, E. E. Ferrero, and J. L. Barrat. Inertia and universality of avalanche statistics: The case of slowly deformed amorphous solids. *Phys. Rev. E*, 95(1):013003, 2017. doi: [10.1103/PhysRevE.95.013003](https://doi.org/10.1103/PhysRevE.95.013003). arXiv: [1610.00533](https://arxiv.org/abs/1610.00533).
- [39] C. P. C. Prado and Z. Olami. Inertia and break of self-organized criticality in sandpile cellular-automata models. *Phys. Rev. A*, 45(2):665–669, 1992. doi: [10.1103/PhysRevA.45.665](https://doi.org/10.1103/PhysRevA.45.665).
- [40] V. H. Purrello, J. L. Iguain, V. Lecomte, and A. B. Kolton. Hysteretic depinning of a particle in a periodic potential: Phase diagram and criticality. *Phys. Rev. E*, 102(2):022131, 2020. doi: [10.1103/PhysRevE.102.022131](https://doi.org/10.1103/PhysRevE.102.022131). arXiv: [2006.04912](https://arxiv.org/abs/2006.04912).